



**HAL**  
open science

## Axial transducer for energy harvesting from galloping

Pascal Hémon, Valentin Bernard, Xavier Amandolese, Maya Hage-Hassan

► **To cite this version:**

Pascal Hémon, Valentin Bernard, Xavier Amandolese, Maya Hage-Hassan. Axial transducer for energy harvesting from galloping. Second International Symposium on Flutter and its Applications, ISFA2020, Xavier Amandolese & Pascal Hémon, May 2020, Paris, France. pp.402 - 411. hal-04390030

**HAL Id: hal-04390030**

**<https://hal.science/hal-04390030>**

Submitted on 12 Jan 2024

**HAL** is a multi-disciplinary open access archive for the deposit and dissemination of scientific research documents, whether they are published or not. The documents may come from teaching and research institutions in France or abroad, or from public or private research centers.

L'archive ouverte pluridisciplinaire **HAL**, est destinée au dépôt et à la diffusion de documents scientifiques de niveau recherche, publiés ou non, émanant des établissements d'enseignement et de recherche français ou étrangers, des laboratoires publics ou privés.



Distributed under a Creative Commons Attribution - NonCommercial - NoDerivatives 4.0 International License

## Axial transducer for energy harvesting from galloping

Maya Hage Hassan<sup>1</sup>, Valentin Bernard<sup>2</sup>, Xavier Amandolese<sup>3,2</sup> and Pascal Hémon<sup>2</sup>

<sup>1</sup> *Université Paris-Saclay, CentraleSupélec, CNRS, Laboratoire de Génie Electrique et Electronique de Paris, 91192, Gif-sur-Yvette, France*

*Sorbonne Université, CNRS, Laboratoire de Génie Electrique et Electronique de Paris, 75252, Paris, France*

<sup>2</sup> *LadHyX, Ecole Polytechnique - CNRS, 91128 Palaiseau Cédex, France*

<sup>3</sup> *LMSSC, Conservatoire National des Arts et Métiers, Paris, France*

### Abstract

In this paper an electromagnetic transducer is optimized to harvest energy from a galloping harvesting system. An electromagnetic modeling of the harvester is firstly proposed by means of Finite Element Analysis (FEA). A comparison with experimental values is done for the model validation. A new transducer is developed to increase the harvesting energy and improve the efficiency. An electromechanical model is developed and validated by means of experimental measurements.

**Keyword:** energy harvesting, transducer, galloping

### 1 Introduction

The transverse galloping phenomenon consists in a self-excited linear oscillation of slender, non-circular structures in a cross flow. One of the earliest analytical description goes back to Den Hartog, who explained this phenomenon in 1943 (Den Hartog, 1985). Recently the idea emerged that the galloping phenomenon could be used for designing an energy harvester from wind or water current. Energy harvesting from transverse galloping has been previously studied analytically by Barrero-Gil et al., (2010) and Vicente-Ludlam et al., (2014). In previous work an energy harvester was presented and described experimentally in Hémon. P et al., (2017).

In this paper, the electromagnetic modelling of this harvester is proposed by means of Finite Element Analysis (FEA). A comparison with experimental values is then realized for the modelling validation. A new transducer is proposed to increase the harvesting energy and improve the efficiency. A Multiphysics model taking into consideration the electromagnetic, electrical and mechanical model is developed. A prototype is tested on the galloping setup to validate both mechanical and electromagnetic model.

The paper is organized as follows: after a short review of galloping, the experimental methodology regarding the measurements, galloping section model set-up are presented in section 2. The modelling and experimental validation of earlier transducer is given in section 3. The design of the new transducer is presented in section 4. Finally, the experimental results are discussed in section 5.

## 2 The galloping phenomenon

Galloping phenomenon is generally referred to be a one degree of freedom instability, in transverse or torsional motion, it can be modeled in the framework of a quasi-static aeroelasticity approximation and using a single-mode oscillator equation for the dynamics of the structure. Considering a square prism with mass  $m$  in a 2-dimensional cross flow supported by a spring with stiffness  $k$  and a damper with damping coefficient  $c$ , the single-mode equation of motion without forcing terms reads as follows:

$$m\ddot{y} + c\dot{y} + ky = 0 \quad (1)$$

If the system is subject to a cross flow, aerodynamic lift and drag forces act on the body. The aerodynamic forces are proportional to the square of the relative flow velocity, that is obtained as the vector sum of the solid and fluid velocity in an inertial reference frame.

$$\vec{u}_{rel} = \vec{u} - \dot{\vec{y}} \quad (2)$$

The drag force acts in the direction of  $\vec{u}_{rel}$  while the lift force acts perpendicular to it. In the reference frame of the section the effect of  $\dot{\vec{y}}$  is a rotation of the incoming flow velocity by an angle  $\alpha = \text{atan}(\dot{y}/u)$ , as seen in Fig. 1. Projecting the aerodynamic forces on the  $y$ -direction of the 2-dimensional plane one obtains the vertical force  $F_y$  that affects the oscillator directly.

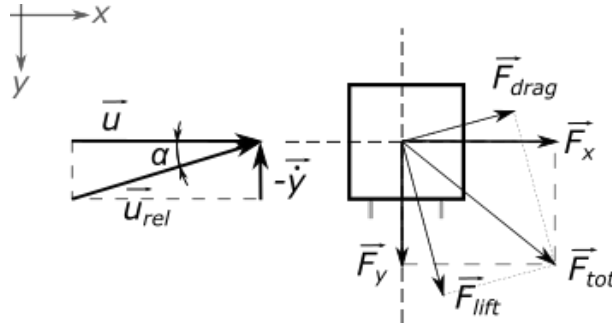


Figure 1: Forces on a section in a cross flow

The magnitude of the force depends on the non-dimensional lift and drag coefficients  $C_l$  and  $C_d$  that are functions of the angle of attack  $\alpha$ .

$$F_l = \frac{1}{2}\rho u_{rel}^2 D l C_l \quad F_d = \frac{1}{2}\rho u_{rel}^2 D l C_d \quad (3)$$

where  $\rho$  is the density of the fluid and  $D$  and  $l$  are the dimension of the prism. Curves for  $C_l$  and  $C_d$  versus angle of attack  $\alpha$  are determined by static wind tunnel experiments and can be found in literature for many cross sections. By projecting the forces onto the  $y$  axis, a combined lift and drag coefficient  $C_y$  can be defined as follows:

$$F_y = F_l \cos(\alpha) + F_d \sin(\alpha) = \frac{1}{2}\rho u_{rel}^2 D (C_l \cos(\alpha) + C_d \sin(\alpha)) \quad (4)$$

$$\Rightarrow C_y = (C_l \cos(\alpha) + C_d \sin(\alpha)) \quad (5)$$

Adding the transverse aerodynamic force to the oscillator equation, the galloping instability is described by the following equation of motion:

$$m\ddot{y} + c\dot{y} + ky = \frac{1}{2}\rho u^2 DIC_y(\alpha) \quad (6)$$

An electromagnetic transducer is studied to harvest the kinetic energy of this galloping structure. In the next section, a brief review of electromagnetic transducers is presented.

### 3 Electromagnetic transducers

Electromagnetic transducers are based on Faraday's law, that states that a variation of the magnetic flux inside a coil, e.g. due to a moving magnet, induces an electromotive force in the coil. The electromotive force ( $e_m$ ) is equal to the time derivative of the flux  $\phi$ :

$$e_m = -\frac{\partial\phi}{\partial t} \quad (7)$$

If the change of flux is only caused by the change of the position  $y$  of a magnet, as is the case in galloping energy harvesting, the electromotive force can be also expressed as:

$$e_m = -\frac{\partial\phi}{\partial y} \frac{\partial y}{\partial t} \quad (8)$$

$-\frac{\partial\phi}{\partial y}$  often is denoted with the name  $k_E$  and represents a coupling coefficient between the magnet and the coil. In most of literature  $k_E$  is considered to be a constant value (El-Hami et al. (2001)). If the coil is integrated into a closed circuit with a load resistance  $R_L$ , the system is described by the following electrical equation :

$$e_m = k_E \dot{y} = L \frac{\partial i}{\partial t} + (R_L + R_i) i \quad (9)$$

Where,  $L$  is the inductance and  $R_i$  the resistance of the harvester coil. The force exerted between the stationary and moving part of the transducer, is given by :

$$F_{em} = k_E i \quad (10)$$

Where  $k_E$  can be calculated using  $NBI$  (El-Hami et al. (2001)). This formulation comes from the simplified case of a square coil of length  $l$  moving from a location without magnetic field into a location with constant magnetic flux density  $B$ . When considering the non-linear behavior of the ferromagnetic material, this coupling coefficient cannot be considered as constant. Since the mechanical system evolves at a much slower time scale than the electronic system, the inductance part of the equation is neglected. Thus the electromechanical coupling system that is considered for the galloping harvester is given by :

$$\begin{cases} m\ddot{y} + c\dot{y} + ky = \frac{1}{2}\rho u^2 DIC_y(\alpha) + k_E(y) i \\ (R_L + R_i) i = k_E \dot{y} \end{cases} \quad (11)$$

While in literature on electromagnetic energy harvesters the Laplace force is the only force appearing in the model, experiments and numerical tests show a strong influence of the static magnetic force in the  $y$  direction between the moving magnets and the stationary core. The influence of this static force can surpass the stiffness force for the used spring at low wind speeds. A static force is determined by *FEA* and added to the model.

#### 4 Energy harvesting device

The electromagnetic transducer used in previous work (Hémon. P et al., (2017)) consists of a coil with 1800 turns, wound around a cylindrical ferromagnetic core of 4 mm diameter and a length of 17 mm. A stack of three neodymium N45 magnets ( $B_r = 1,320$  T,  $H_{cJ} = 923$  kA/m) with dimensions  $5 \times 10 \times 3$  mm where mounted on the galloping set-up, and the coil was placed in front of the magnets Fig. 2. The magnets are located on the suspension beams that ensure the vertical stiffness of the aeroelastic system.

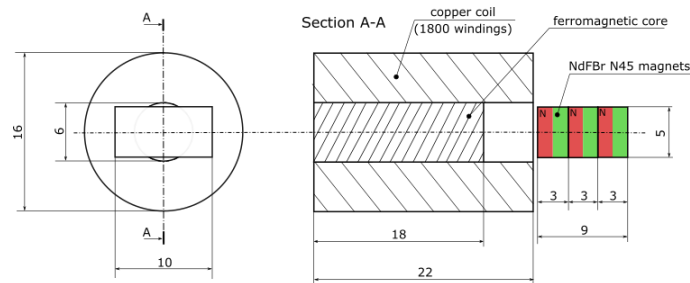


Figure 2: Drawing of the first transducer model

The magnet-coil-combination was modelled by means in 2D FEA using *FEMM*, as presented in Fig. 3 the flux lines due to NdFeB magnetic field are not optimally used, the flux is not totally enclosed in the ferromagnetic circuit to improve the electromotive force (emf).

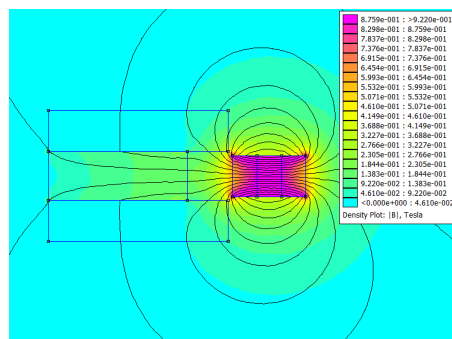


Figure 3: Flux direction and flux density of the magnetic field in the transducer (*FEMM* result)

For the given transducer,  $k_E$  is determined through a magnetostatic analysis using *FEMM* tool. The variation of  $k_E$  as function of magnets' position is given in Fig. 4. The calculation has been performed in a motion range of 50 mm from the equilibrium position in both directions, obtaining a curve for  $k_E$  as a function of the magnet position  $y$ .

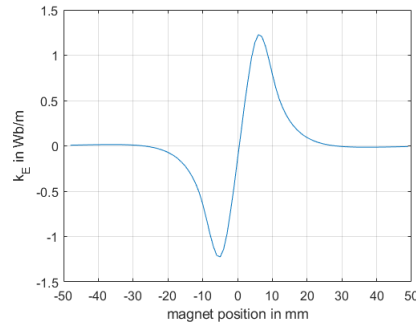


Figure 4: Result for  $k_E$  at every position of the magnet

To validate the proposed model, the  $k_E(y)$  curve has been inserted into a *Simulink* model for the differential equation governing the circuit of the transducer and it is proposed to reconstruct the graph given in Fig. 5 the measured output voltage is at a load resistance of 80 . The same motion was imposed in the *Simulink* model, and the resulting voltage was observed. As can be seen in Fig. 5, the model can predict with high accuracy the shape of the output voltage.

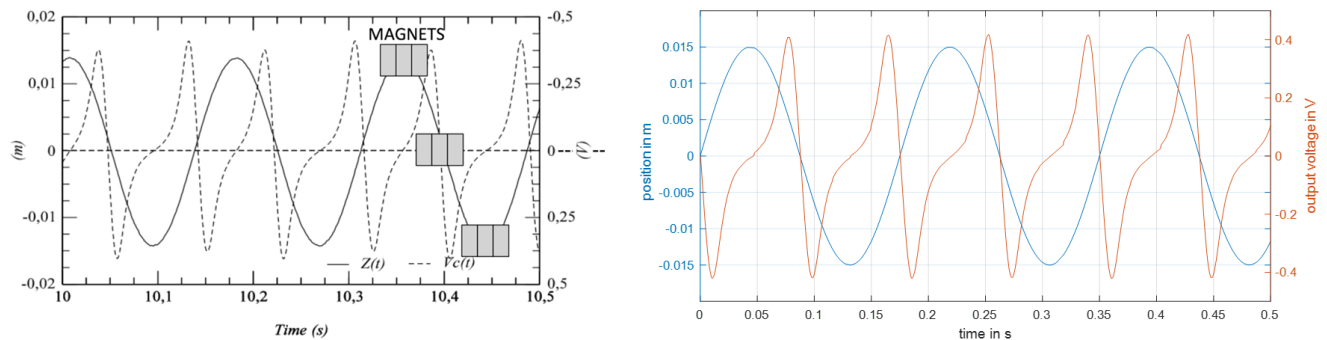


Figure 5: Left: experimental results obtained previously, right: results of the *Simulink* model

#### 4.1 New proposals

New transducer designs are proposed and tested in simulation. The design are based on standardized E-shaped laminates in ferromagnetic FeCo material. A drawing of the proposal is shown in Fig. 6. It consist a coil wound around the central leg of an E-shaped core pieces, assembled from laminates. Three magnets are mounted on a ferromagnetic support with an air gap of 1 mm to the core. NdFeBr magnets with coercivity  $H_c = 1042$  kA/m are chosen. These magnets are commonly sold under the name N45SH in the Chinese standard nomenclature. The design is meant to create a closed magnetic circuit in order to have maximum flux variation inside the coil, and therefore increase the output voltage.

The second proposal is similar to the first one, but aims to double the number of winding affected by the flux variation. A second E-shaped core with a coil on the central leg is placed in face of the first one. The magnets are now longer mounted on a ferromagnetic core, and are moving inside the air gap between the two cores. Dimensions and magnets are the same as in the single E proposal. Fig. 7 shows the *FEMM* model of this second proposal.

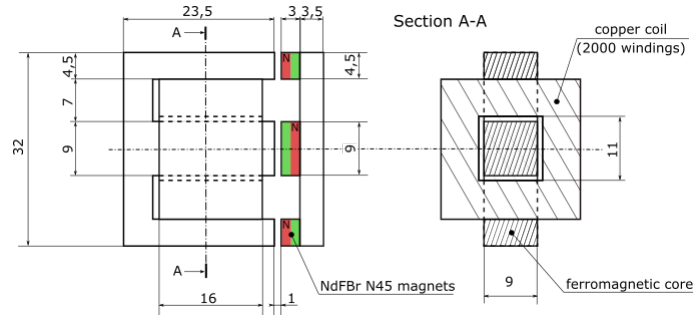


Figure 6: Single E transducer

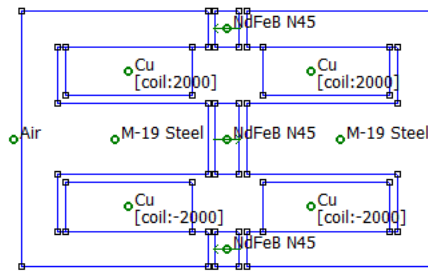


Figure 7: Double E transducer *FEMM*

When compared the single E proposal increases the  $k_E$  value by a factor of 25 and that of double-core proposal by a factor of 45 (Fig. 8).

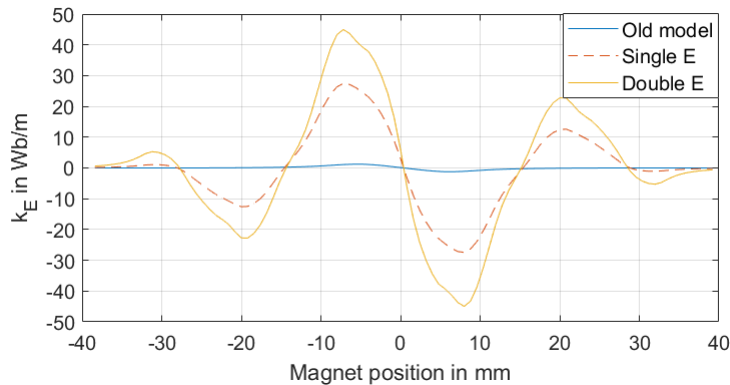


Figure 8: Comparison of  $k_E$  curves for the three transducers

In order to select the optimal transducer for this application, the global efficiency of the system is determined as function of the load resistance. Where it was defined as the ratio between the mechanical energy flowing across the swept area of the galloping beam and the electrical energy dissipated in the load resistance.

$$\mu = \frac{i_{rms}^2 R_L}{\frac{1}{2} \rho u^3 l (D + 2\hat{y})} \quad (12)$$

Where,  $I(D + 2\hat{y})$  represents the area swept by the beam during its motion. Fig. 9 shows how the load resistance affects the efficiency of the harvester using the described transducers. The result show a strong effect of the load resistance. Fig. 10 gives the efficiency that can be obtained when optimizing the load resistance at every reduced velocity, as well as the resistance value that is found to be optimal according to the model.

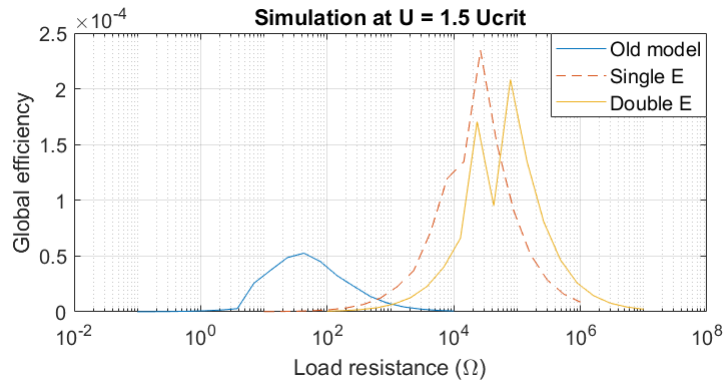


Figure 9: Effect of the load resistance on the efficiency of the harvester using three different transducers

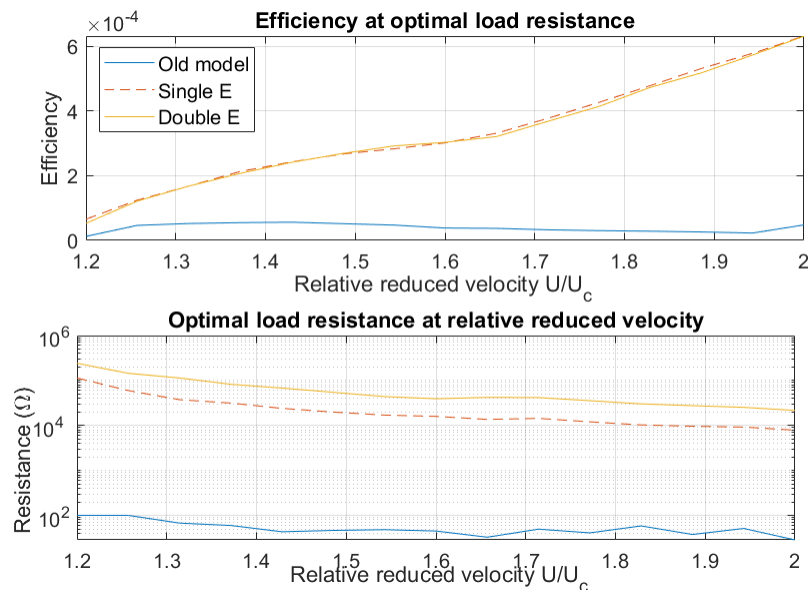


Figure 10: Efficiency achieved when using the optimal load resistance at each reduced velocity

Using this energy conversion chain, the efficiency of the single subsystems can be defined, it is found that the bulk of the inefficiency is due to the aerodynamics of the galloping phenomenon. In the range of parameters tested with the model, no more than 0.1% of the energy available in the wind are converted into mechanical energy in the oscillator. This is coherent with previous experimental results (Hémon. P et al., (2017)). From efficiency results, the single side E is selected to be experimentally validated.



## 5 Experimental validation

The magnet support is fixed onto the galloping beam, while the core with the coils is mounted on a linear guide that allows the transducer to be placed at any air gap between 1 mm and 20 mm. The air-gap of 5mm was chosen in order to minimize the static forces.

A new galloping set-up has been built, based on the set-up tested in (Hémon. P et al., (2017)). The set-up, shown in Fig. 11 consists in a square beam of length  $l = 250$  mm and width  $D = 17$  mm. Square plates made from Plexiglas are attached flat on both ends of the beam. This is meant to keep the flow 2-dimensional. This assembly is placed inside a closed loop wind tunnel. The assembly is suspended by one laminar and two linear springs both sides. No other constraining elements are used, in order to minimize the structural damping of the set-up.

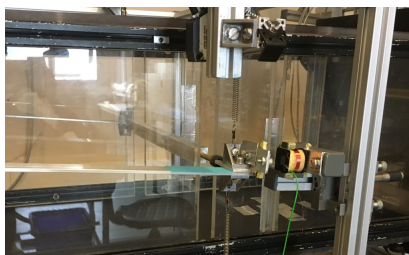


Figure 11: Experimental Set-Up

As for the transducer (Fig. 12), the coil was wound from 0.1 mm copper wire and contains 2000 windings. The resulting internal resistance of the coil  $R_i$  is 266  $\Omega$ . As for the core it's made of laminated iron.

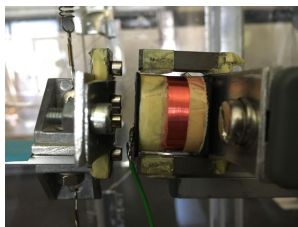


Figure 12: Photograph of the experimental transducer

The magnet support is fixed onto the galloping beam, while the core with the coils is mounted on a linear guide that allows the transducer to be placed at any air gap between 1 mm and 20 mm. The air-gap of 5mm was chosen in order to minimize the static forces.

In order to validate the correctness of the electromagnetic model of the transducer, the galloping set up with engaged transducer was tested at several wind speeds, recording the limit cycle oscillatory motion as well as the exact shape of the voltage on the load resistance. This data could then be compared to the voltage shape predicted by the model at that particular motion of the magnets to validate the transducer model. The validation was performed using a model that does not compute the aerodynamics and considers the motion of the oscillator as given. The experiment has been performed at wind speeds close to the critical velocity,

where the galloping model was expected to give good results for the motion. Wind speeds of 4.49 m/s and 5.66 m/s were chosen. To validate the model of the electromagnetic transducer, and in particular  $k_E$ , oscillations have been recorded and imposed on the model, comparing the resulting voltage to the measured voltage. When the approximation for small impedance is applied to equation 9, one obtains the following equation for the output voltage  $V_{out}$ :

$$V_{out} = \frac{R_L}{R_i + R_L} k_E \dot{y} \quad (13)$$

Voltage shape for a given motion is therefore a direct validation for the  $k_E$  curve that was computed using *FEMM*. Various motion aptitudes have been tested by applying setting wind speeds. A load resistance of 500  $\Omega$  was chosen for all wind speeds. The recorded motion has been converted into a time signal and imposed on a *Simulink* model that contains only the transducer, and disregards all the mechanics, must taking a forced motion as input. The results for various wind speeds can be seen in Fig. 13.

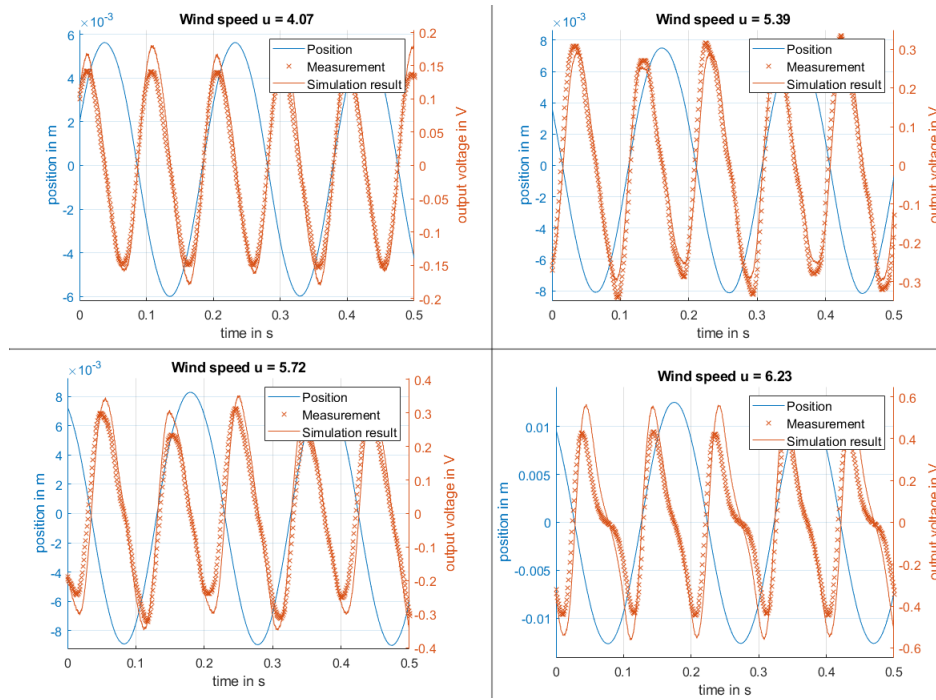


Figure 13: Measured and simulated voltage at different wind speeds.

In all cases, the model correctly predicts the output voltage. In terms of accuracy of the predicted amplitude, the results seem to vary between different measurements. This can be due to the used *BH curve* of the ferromagnetic part, and the equivalent depth of the circular magnets used in *FEMM*.

Experiments to determine the optimal load resistance have been carried out at two wind speeds, with the transducer set at an air gap of 5 mm. Wind speeds were chosen low to remain in the area where the predictions of the galloping model are more accurate. The results for measured efficiency at  $u = 5.66$  m/s are given in Fig. 14. The model largely overestimates the motion amplitude as well as the efficiency. The amplitude is predicted to be about 3 times larger than the experiment for high load resistances, with a decreasing difference for lower  $R_L$ .

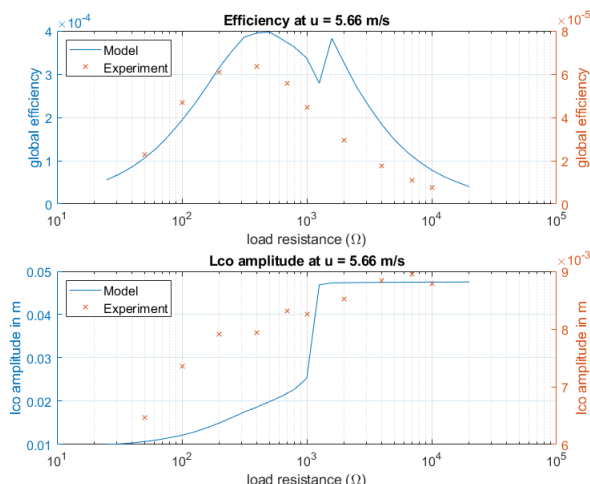


Figure 14: Measured and simulated efficiency and lco amplitude at wind speed of 5,66 m/s

## 6 Conclusion

In this paper an axial transducer is proposed to harvest energy from galloping. A multiphysics model of the transducer was able to predict the shape and amplitude of the output voltage given an input signal with reasonable precision. As for future work, an optimization of the geometry of the harvester could be performed. It might be interesting to inverse the design approach for the harvester and starting from a desired  $k_E$  vs  $y$  curve, an optimized transducer is proposed.

## References

- M. P. Paidoussis, S. J. Price, and E. De Langre, Fluid-structure interactions: cross-flow-induced instabilities. Cambridge University Press, 2010
- Den Hartog, J.P., 1985. Mechanical Vibrations. Reprint of the 1934 edition. Dover, New York
- Barrero-Gil, A., Alonso, G., Sanz-Andres, A., 2010. Energy harvesting from transverse galloping. J. Sound and Vibration 329, 2873-2883.
- Vicente-Ludlam, D., Barrero-Gil, A., Velazquez, A., 2014. Optimal electromagnetic energy extraction from transverse galloping. J. Fluids and Structures 51, 281-291.
- Padoussis, M. P., 2016. Dynamics of tubular cylindrical structures in axial flow. In: Proceedings of the first International Symposium on Flutter and its Application, Paper ISFA-1K01, Tokyo, Japan.
- Sears, W.R., 1941. Some aspects of non-stationary airfoil theory and its practical application. Journal of the Aeronautical Sciences 8, 104-108.
- Hémon. P., Amandolese. X. and Andrienne. T., Energy harvesting from galloping of prisms: A wind tunnel experiment," Journal of Fluids and Structures, vol. 70, pp. 390402, 2017.
- El-Hami, M., Glynne-Jones, P., White, N., Hill, M., Beeby, S., James, E., Brown, A. and Ross, J., Design and fabrication of a new vibration-based electromechanical power generator," Sensors and Actuators A: Physical, vol. 92, no. 1-3, pp. 335-342, 2001.